Integrated Photonics for Computing, Interconnects and Sensing

Jason Midkiff[1], Ali Rostamian[1], Kyoung Min Yoo[1], Aref Asghari[1], Chao Wang[1], Chenghao Feng[1], Zhoufeng Ying[1], Jiaqi Gu[1], Haixia Mei[1], Ching-Wen Chang[1], James Fang[2], Alan Huang[2], Jong-Dug Shin[2], Xiaochuan Xu[2], Michael Bukshtab[2], David Pan[1], and Ray T. Chen[1,2]

[1]Microelectronics Research Center
The University of Texas, Austin
10100 Burnet Rd., Building 160
Austin, TX 78758

[2]Omega Optics Suite 200
8500 Shoal Creek Blvd.
Austin, TX 78757
chenrt@austin.utexas.edu

Integrated photonics is poised to revolutionize inter- and intra-data center communications since internet traffic continues to increase exponentially making it difficult and costly for existing switching and interconnects in data centers to cope with the ever-increasing bandwidth requirement. As many fundamental components including power-efficient modulators are maturing, integrated photonics is believed to be reaching a tipping point with the surging global market. Besides clear contributions to optical interconnects, integrated photonics also shows promise in a variety of diverse applications such as high-performance optical computing and lidar for autonomous cars, biomedical sensing, and even aerospace applications.

In the context of our group's research, this talk provides an overview of the current state of integrated photonics as well as potential trends for the next decade. We present recent developments in selected optical components—including both passive and active modules—as well as optical circuits in both silicon and III-V-based systems. As Moore's law has been approaching its physical limit, photonics-based high-performance computing is envisioned as a potential answer to its extension [1]. We propose and experimentally demonstrate a new photonics-assisted full adder which is capable of operating at a higher frequency than its electrical counterparts while consuming less power [2]. This demonstration paves the way to future integrated high-speed, power-efficient optical computing. In the realm of sensing, we present progress in both lab-on-chip and lidar-based sensing. For lab-on-a-chip sensing, the biomarkers we report so far include those of breast, lung, and pancreatic cancers, three antibiotic drugs, and a few heavy metals. For spectroscopic lidar-based sensing we target hazardous gaseous analytes including chemical warfare agents and greenhouse gases.

The basic concept of lab-on-a-chip sensing is shown in Figure 1. The system consists of three main components—bioreceptor, optical transducer, and data processor. Numerous bioreceptor-target coupling strategies are employed, the optimization of such couplings being critical for maximum sensitivity and accuracy.

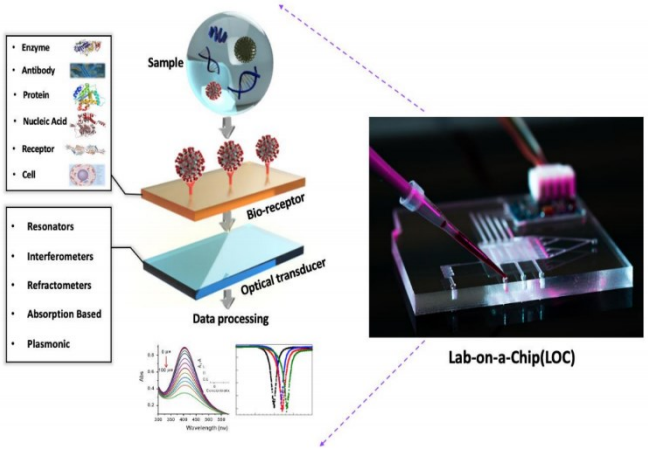

Figure 1: Schematic working principle of a lab-on-a-chip (LOC) optical biosensor.

Our optical transducer for biosensing is a microring resonator, shown in Figure 2. By forming the waveguide of sub-wavelength grating metamaterial (SWGM), unprecedented sensitivity to femto-mole concentration levels on a myriad of biomarkers is achieved without sacrificing specificity [3]. The surface sensitivity S_s is defined as:

$$S_s = \frac{\Delta\lambda}{\Delta t} = \frac{\lambda}{n_g}\left(\frac{\partial n_{eff}}{\partial t}\right), \qquad (1)$$

where $\Delta\lambda$ is the resonance wavelength shift, Δt is the change of surface layer thickness, ∂n_{eff} is the effective refractive index of the waveguide mode, and n_g is the group index. Following H. Yan *et al.* simulation and experimental results, the large mode overlap factor provides 4-6 times higher $\frac{\partial n_{eff}}{\partial t}$ in the SWGM microring resonator in comparison to a traditional strip

waveguide microring resonator [4]. Hence the SWGM microring resonator can provide superior surface sensitivity and greater sensing capability in comparison with a regular strip waveguide microring resonator.

A fully automated portable optical bio-sensing system based on the SWGM microring resonator has been successfully demonstrated. The open biosensing platform has attained a Technology Readiness Level of 6. The graphic user interface written in MATLAB for system manipulation is designed with ease of use in mind. The real-time relative resonance peak shifts of the resonator observed for streptavidin detection exemplifies the excellent system performance.

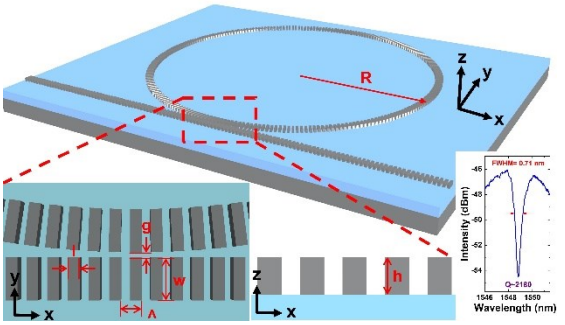

Figure 2: Schematic of SWGM waveguide microring resonator. R is the diameter of the microring, Λ is the subwavelength grating period, h is the thickness of waveguide core, w is the width of waveguide core, l is the length of silicon pillar, and g is the gap between microring and bus waveguide. The right-bottom insert shows the transmission spectrum of the fabricated microring.

The same open biosensing platform can also be employed for COVID-19 detection with the integration of a microfluidic channel for saliva-based specimens [5]. Label-free microarrays are particularly exciting because they simplify the biochemistry significantly—probe-target binding conjugations can be studied without the steric hindrance associated with fluorescent or radioactive tags. We have employed photonic crystal (PC) microarrays for high sensitivity to small changes in concentration. The architecture also lends itself to dense integration due to its small geometric size.

For lidar-based spectroscopic sensing applications, we present a beam steering device for operation in the first mid-IR atmospheric window. Fabricated in the InGaAs/InP platform, the device is a steppingstone to monolithic integration with mid-IR quantum cascade sources for small, lightweight, power-efficient modules. Figure 3 shows our optical phased array device [6]. Future mid-IR lidar systems will enable remote sensing of industrial, war-derived, and environmentally hazardous gases.

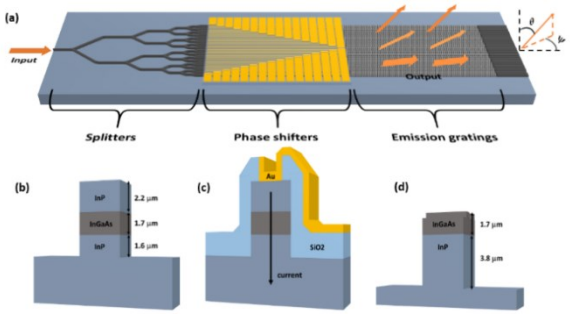

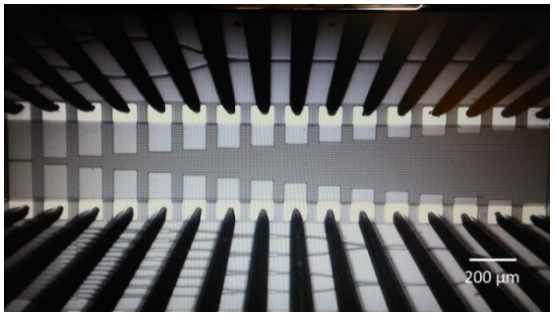

Figure 3: Schematic illustration of an InP-based optical phased array. (a) Entire layout with input and output light indicated. (b), (c), and (d) Cross-sections of the ridge waveguide structure in the splitter, phase shifter, and emission gratings regions, respectively. (e) Microscope photo of 32 phase shifters contacted by probes.

References

1. Ray Chen, *et al*., Proc. IEEE 88, p.780-793 (2000).
2. Zhoufeng Ying, *et al*., Nat. Commun. 11, 2154 (2020).
3. Varun Soni, *et al*., IEEE Trans. Biomed. Eng. 68, 6, p. 1894-1902 (2021).
4. H.Yan *et al.*, Opt. Express 24, 26, p. 29724 (2016).
5. Aref Asghari, *et al*., arXiv:2008.08572 (2020).
6. Jason Midkiff, *et al*., Optica 7, 11, p. 1544-1547 (2020).